SOILS AND FOUNDATIONS Vol. 49, No. 6, 853–869, Dec. 2009
Japanese Geotechnical Society

DISPLACEMENT-BASED DESIGN OF SHALLOW FOUNDATIONS WITH MACROELEMENT

C. T. CHATZIGOGOS[i], A. PECKER[ii] and J. SALENÇON[iii]

ABSTRACT

The scope of this paper is to demonstrate the utility of macroelement modeling of shallow foundations in performance-based design. We focus on the settlements, horizontal displacements and rotations of a bridge pier founded on a rigid circular foundation on a relatively soft cohesive soil. A newly developed macroelement model is used for the description of the footing-soil system. Its objective is to reproduce the geometric (uplift of the footing) and material non-linearities (soil plasticity) that arise at the foundation level during a seismic excitation. The utility of macroelement modeling resides in the fact that it allows for the execution of a large number of non-linear dynamic analyses of the pier under the horizontal and vertical components of real acceleration time histories as well as under the combination of both. The results concentrate on two main points: the influence of the vertical component of the seismic input motion on the maximum and residual displacements of the foundation and on a discussion of possible correlations between the induced displacements at the foundation level and certain parameters describing the severity of the seismic input motion.

Key words: macroelement modeling, non-linear dynamic analysis, performance-based design, plasticity models, residual displacements, shallow foundations (**IGC**: E8/H1)

INTRODUCTION

This paper aims at demonstrating the utility of the concept of macroelement in performing parametric investigations of the non-linear dynamic response of shallow foundations with a particular orientation towards performance-based design. The newly developed macroelement model presented by Chatzigogos et al. (2008) is used in an effort to establish correlations between the earthquake-induced displacements at the foundation level of a bridge pier and some characteristic quantities describing the earthquake input excitation.

The paper is divided in two parts. In the first part, a brief description of the macroelement model is recalled while a more complete presentation can be found in Chatzigogos (2007) and in Chatzigogos et al. (2008). In the second part, a large number of non-linear dynamic analyses using the macroelement are performed. They concentrate on two main objectives: a) to investigate the influence of the vertical component of the seismic input motion on the response of the foundation and b) to determine which parameters of the considered acceleration time histories satisfactorily correlate with the computed displacements at the foundation level.

The large utility of the macroelement resides in the fact that it allows for an efficient execution of the proposed analyses that would otherwise require a tremendous computational cost if the soil and the foundation were to be explicitly modeled most commonly with a finite element mesh.

PRESENTATION OF THE MACROELEMENT MODEL

A Short Survey of Existing Macroelement Models

As it arises in the context of earthquake-resistant design of foundations, the concept of ''***macroelement***'' consists in replacing the entire foundation-soil system by a single element placed at the base of the superstructure and aiming at reproducing the non-linear soil-structure interaction effects that take place at the foundation level (cf. Fig. 1(a)). These may be of a ''material'' origin as the irreversible dissipative soil behavior or of a ''geometric'' origin as the phenomenon of uplift that may take place at the soil-footing interface. Taking into account these non-linearities is a key aspect of the performance/displacement-based design philosophy: we allow the structure (i.e., the foundation – soil system) to enter into a non-linear regime, achieving a less expensive design, but we have to guarantee that the induced displacements pertain-

[i] Laboratoire des Matériaux et des Structures du Génie Civil, ENPC, France (charisis.chatzigogos@wanadoo.fr, charisis.chatzigogos@lmsgc.enpc.fr).
[ii] Professor of the École Nationale des Ponts et Chaussées, France.
[iii] Professor Emeritus of the École Polytechnique, France.
The manuscript for this paper was received for review on January 25, 2008; approved on December 16, 2008.
Written discussions on this paper should be submitted before July 1, 2010 to the Japanese Geotechnical Society, 4-38-2, Sengoku, Bunkyo-ku, Tokyo 112-0011, Japan. Upon request the closing date may be extended one month.

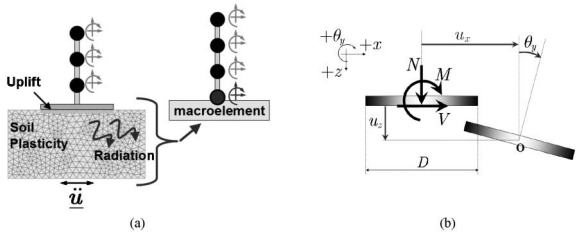

Fig. 1. (a) Definition of the concept of macro-element and (b) Forces and corresponding kinematic parameters for a shallow perfectly rigid footing

ing to the performance of the structure will not exceed some prescribed limits.

The description of the aforementioned non-linearities is achieved in a phenomenological way within the macroelement through a non-linear ''constitutive law'' linking the increment of some generalized force parameters to the increment of the corresponding kinematic parameters. The generalized force and displacement parameters are chosen in such a way so as to be consistent with those adopted for the superstructure model and their definition is rendered straightforward if the foundation is considered perfectly rigid. Moreover, the formulation of the model is facilitated if these parameters are introduced dimensionless. In the following, we will present a macroelement model for a shallow, perfectly rigid, circular footing for which, we introduce the following scheme of dimensionless generalized forces and displacements (cf. Fig. 1(b)):

$$\underline{Q}^{\mathrm{T}} = [Q_{\mathrm{N}} \;\; Q_{\mathrm{V}} \;\; Q_{\mathrm{M}}] = \frac{1}{N_{\max} D} [ND \;\; VD \;\; M] \tag{1}$$

$$\underline{q}^{\mathrm{T}} = [q_{\mathrm{N}} \;\; q_{\mathrm{V}} \;\; q_{\mathrm{M}}] = \frac{1}{D} [u_z \;\; u_x \;\; D\theta_y] \tag{2}$$

In Eqs. (1), (2) D is the footing diameter, $N_{\max}$ is the maximum vertical force supported by the footing under vertical centered load, N, V and M are the resultant vertical and horizontal force and moment on the footing, u_x, u_z are the horizontal and vertical displacement of the footing center respectively and θ_y is the rotation angle of the footing.

Several macroelement models for rigid shallow foundations have already appeared in the literature (cf. Table 1). In almost all cases, the modeling procedure is initiated by the determination of the ***surface of ultimate loads*** that can be supported by the foundation, in the space of the generalized forces. Once this surface has been identified (by either experimental or theoretical procedures), it is used as a ***yield surface*** for the formulation of a plasticity model written in terms of Q_i and $\dot{q}_i$. The model is supplemented with a heuristically defined flow rule (usually non-associated) that provides the best fit to the observed footing behavior. The features of the model are prescribed according to the context of application, which is commonly either off-shore or earthquake-resistant foundation design. The sophistication of the plasticity model may vary from an elastic perfectly plastic formulation to advanced models with kinematic/isotropic hardening derived within a thermodynamically consistent framework. For applications in earthquake engineering, efforts have been presented to introduce a description of uplift and to couple it with the plasticity model. From a theoretical perspective, macroelement formulations have also been derived analytically based on the Winkler hypothesis of uncoupled contact-breaking elastoplastic springs attached at the soil-footing interface.

Table 1 presents a non-exhaustive overview of several existing macroelement models for shallow foundations.

Scope of the Model – Modeling Principles

The model presented in the paper is developed for earthquake engineering applications. As such, it is desirable that it accounts for both the material and the geometric non-linearities (plasticity and uplift) of the real system in a coupled way. It consists in two mechanisms distinct from each other in order to take into account both non-linearities listed above: an elasto-plastic model and a non-linear elastic model. As a consequence, what may appear as the main originality with respect to all previous models is that the yield surface of the elasto-plastic model (actually its bounding surface, cf. *Plasticity Model*) is different from the surface of ultimate loads of the foundation. This is not surprising because of the presence of uplift; the surface of ultimate loads of the foundation is a combined result of both plasticity and uplift.

The model is formulated with respect to the configuration presented in Fig. 2. The rigid circular foundation is resting on a soft cohesive homogeneous and isotropic soil with unit weight γ obeying the classical Tresca strength criterion with cohesion c. Its elastoplastic constitutive equation is described by an associated flow rule. The soil-footing interface will be considered perfectly rough with zero tensile strength so that it allows for uplift. Considering the horizontal plane directly below the footing in a σ-τ diagram, we obtain the combinations of (σ, τ) that are admissible in the system. The following remarks are retained:

a. The first thing to be determined is the surface of ultimate loads of this system. Every loading state predicted by the macroelement model must lie in the interior of this surface. Anticipating the modeling procedure, it is clear that the selection of the macroelement parameters must invariably comply with this criterion whatever the origin of the parameters. For the examined configuration, the surface of ultimate loads has been determined in Chatzigogos et al. (2007).

b. The elastoplastic soil behavior will induce the first non-linearity to be included into the ''constitutive law'' of the macroelement: it is an irreversible dissipative mechanism that will be described by a plasticity model written in terms of the generalized force and kinematic parameters Q_i-q_i.

c. The interface conditions allowing for uplift will induce the second non-linear mechanism for the macroelement: it will be totally reversible and non-dissipative and

Table 1. Overview of existing macroelement models for shallow foundations

Reference	Year	Configuration	Description
Nova & Montrasio	1991	Strip footing resting on a purely frictional soil	Isotropic hardening plasticity model and non-associated flow rule. Application in the case of quasistatic monotonic loading.
Paolucci	1997	Strip footing resting on a purely frictional soil	Perfect plasticity model with non-associated flow rule. Application to simple structures subject to seismic loading. Parametric studies.
Pedretti	1998	Strip footing resting on a purely frictional soil	Hypoplastic model for the description of the system response under cyclic loading. Consideration of uplift by reduction of the elastic stiffness. Applications to structures subject to quasistatic cyclic loading.
Gottardi et al.	1999	Strip footing resting on a purely frictional soil	Isotropic hardening plasticity model. Detailed description of the system ultimate surface (identified as the yield surface of the plasticity model) via ''swipe tests''. Application in the case of quasistatic monotonic loading.
Le Pape et al. Le Pape & Sieffert	1999 2001	Strip footing resting on a purely frictional soil	Elastoplastic model derived from thermodynamical principles. Rugby-ball shaped yield surface and ellipsoidal plastic potential. Application to seismic loading.
Crémer et al.	2001, 2002	Strip footing resting on a purely cohesive soil without resistance to tension	Non-associated plasticity model with isotropic and kinematic hardening coupled with a model for uplift. Application to seismic loading.
Martin & Houlsby	2001	Circular footing resting on a purely cohesive soil	Non-associated plasticity model with isotropic hardening. Detailed description of the yield surface via ''swipe tests''. Application to quasistatic monotonic loading.
Houlsby & Cassidy	2002	Circular footing resting on a purely frictional soil	Non-associated plasticity model with isotropic hardening. Detailed description of the yield surface via ''swipe tests''. Application to quasistatic monotonic loading.
Di Prisco et al.	2003	Strip footing resting on a purely frictional soil	Hypoplastic model for the description of the behavior under cyclic loading. Application to quasistatic cyclic loading.
Cassidy et al.	2004	Circular footing resting on a frictional or cohesive soil	Fully three-dimensional formulation. Application to the off-shore industry. Quasistatic monotonic loading.
Houlsby et al.	2005	Strip or circular footing resting on cohesive soil. Frictional soil-footing interface	Decoupled Winkler springs with elastic perfectly plastic contact-breaking law derived from thermodynamical principles. Application to quasistatic cyclic loading.
Einav & Cassidy	2005	Strip footing resting on cohesive soil. Frictional soil-footing interface	Decoupled Winkler springs with elastoplastic contact-breaking law with hardening derived from thermodynamical principles. Application to quasistatic cyclic loading.
Gajan & Kutter	2007	Strip footing	Moment – rotation and settlement – rotation relationship obtained by tracking the contact area at the soil-footing interface. Extensive experimental validation.
Grange et al.	2008	Circular footing on cohesive soil	Extension of the plasticity model of Crémer to purely three-dimensional setting. Uplift modeled as a second plasticity mechanism.

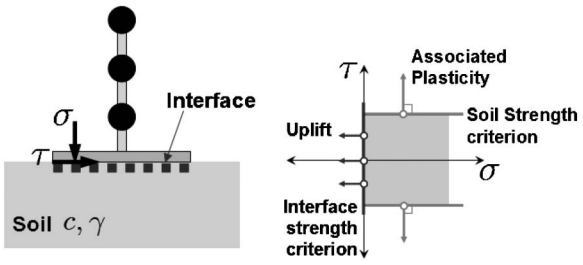

Fig. 2. Examined configuration for soil and soil-footing interface. The soil strength criterion induces in the macroelement scale the non-linear mechanism of soil plasticity. Similarly, the interface criterion induces in the macroelement the non-linear mechanism of uplift. Note that plasticity is dissipative while uplift takes place with zero dissipation

it can thus be described by a phenomenological non-linear elastic model complying with its reversible and non-dissipative character.

d. The maximum vertical force supported by the system (for use in (1)) is computed by the following equation (cf. Eason and Shield, 1960):

$$N_{\max} = 6.06c\,\frac{\pi D^2}{4} \tag{3}$$

e. The two mechanisms (plasticity – uplift) will initially be introduced into the macroelement formulation independently from each other. This will allow obtaining an individual mechanism if the other is deactivated (plasticity without uplift or uplift without plasticity).

f. Once the two mechanisms have been introduced into the macroelement formulation, it will be easier to define the elements of coupling between them.

g. Formulation of the model will be obtained with reasoning in terms of *total stresses* within the soil. This assumption complies with the consideration of a cohesive soil under earthquake loading and implies that the soil is not susceptible to liquefaction.

Proceeding according to remark (e), we formulate the uplift model by considering a circular footing uplifting

Table 2. Approximate relationships for the static impedances and the radiation damping coefficients (dimensional) of a circular footing resting on homogeneous elastic half-space

Mode	Static Impedances	Radiation damping coefficients
Vertical	$\tilde{K}_{NN}=\frac{2GD}{1-\nu}$	$C_{NN}=\rho V_{La}\left(\frac{\pi D^2}{4}\right)$
Horizontal	$\tilde{K}_{VV}=\frac{4GD}{2-\nu}$	$C_{VV}=\rho V_{S}\left(\frac{\pi D^2}{4}\right)$
Rotational	$\tilde{K}_{MM}=\frac{GD}{3(1-\nu)}$	$C_{MM}=\rho V_{La}\left(\frac{\pi D^4}{64}\right)$

on an elastic half-space (no plasticity) and the plasticity model by considering a circular footing perfectly bonded to the surface of an elastoplastic soil (no uplift).

Non-linear Elastic Model for the Uplift Mechanism

For the formulation of the uplift model we examine the case of a perfectly rigid circular footing that can be detached from the surface of an elastic half-space.

Before uplift initiation, the response is linear and the forces Q_i may be linked to the elastic displacements q_i^{el} through a constant stiffness matrix with coefficients $\tilde{K}_{ij}$ (we use the wide tilde to denote the elements of the elastic stiffness matrix before uplift initiation). It has been shown that for shallow footings with planar base (cf. Veletsos and Wei, 2001) the off-diagonal terms $\tilde{K}_{ij}$, $i\neq j$ are negligible, so one can write:

$$\begin{bmatrix} Q_N \\ Q_V \\ Q_M \end{bmatrix} = \begin{bmatrix} \tilde{K}_{NN} & 0 & 0 \\ 0 & \tilde{K}_{VV} & 0 \\ 0 & 0 & \tilde{K}_{MM} \end{bmatrix} \begin{bmatrix} q_N^{el} \\ q_V^{el} \\ q_M^{el} \end{bmatrix} \tag{4}$$

In Eq. (4) and for the case of quasi-static loading, the terms $\tilde{K}_{ii}$ can be identified with the static impedances of the foundation. These are functions of the elastic properties of the soil (G: shear modulus, ν: Poisson's ratio) and of the foundation geometry. Approximate relationships for these quantities are reported in Gazetas (1991) and are presented in Table 2.

Uplift is initiated once the applied moment on the footing $|Q_M|$ exceeds (in absolute value) a certain value which will be denoted $Q_{M,0}$. This quantity is a function of the footing geometry and is linear with respect to the applied vertical force:

$$Q_{M,0}=\pm\frac{Q_N}{\alpha} \tag{5}$$

The dependence upon footing geometry is expressed through the parameter α. For strip footings, $\alpha=4$ (cf. Crémer et al., 2001, 2002) while for circular footings $\alpha=6$ (cf. Wolf, 1988). The elastic stiffness matrix during uplift can be calibrated using results from finite element analyses. The case of strip footings has been covered by Crémer et al. (2001, 2002). Similarly, the case of circular footings has been treated in Wolf (1988). The results have been obtained by fixing the applied vertical force on the footing and then increasing the applied moment until toppling of the structure. Moreover, the common assumption will be adopted that uplift has no effect on the behavior of the system under horizontal loading.

Table 3. Values of the numerical parameters in Eqs. (5)–(7)

	α	β	γ	δ	ε
STRIP	4	2	1	1	$\frac{1}{2}$
CIRCULAR	6	3	2	$\frac{1}{2}$	$\frac{3}{4}$

Chatzigogos et al. (2008) have shown that the results for either strip or circular footings can be expressed through two approximative relationships obtained with curve fitting:

$$\frac{Q_M}{Q_{M,0}}=\beta-\gamma\left(\frac{q_{M,0}^{el}}{q_M^{el}}\right)^{\delta} \tag{6}$$

$$\frac{\dot{q}_N^{el}}{\dot{q}_M^{el}}=-\varepsilon\left(1-\frac{q_{M,0}^{el}}{q_M^{el}}\right) \tag{7}$$

In Eq. (6), the quantity $q_{M,0}^{el}=\tilde{K}_{MM}^{-1}Q_{M,0}$ expresses the rotation angle at uplift initiation. Eq. (6) provides the moment – rotation diagram after uplift has been initiated and Eq. (7), the coupling between the vertical force and moment during uplift. Parameters β, γ, δ, ε are numerical constants that depend on footing geometry. Their values for strip and circular footings are given in Table 3.

Using Eqs. (5)–(7), the symmetry of the stiffness matrix and assuming that the term K_{NN} remains constant and equal to $\tilde{K}_{NN}$ even after uplift initiation, the following non-linear elastic stiffness matrix is obtained:

$$\begin{bmatrix} \dot{Q}_N \\ \dot{Q}_V \\ \dot{Q}_M \end{bmatrix} = \begin{bmatrix} K_{NN} & 0 & K_{NM} \\ 0 & K_{VV} & 0 \\ K_{MN} & 0 & K_{MM} \end{bmatrix} \begin{bmatrix} \dot{q}_N^{el} \\ \dot{q}_V^{el} \\ \dot{q}_M^{el} \end{bmatrix} \tag{8}$$

with:

$$K_{NN}=\tilde{K}_{NN} \tag{9}$$

$$K_{VV}=\tilde{K}_{VV} \tag{10}$$

$$K_{MN}=K_{MN}=\begin{cases} 0, & \text{if} \quad |q_M^{el}|\leq|q_{M,0}^{el}| \\ \varepsilon K_{NN}\left(1-\frac{q_{M,0}^{el}}{q_M^{el}}\right), & \text{if} \quad |q_M^{el}|>|q_{M,0}^{el}| \end{cases} \tag{11}$$

$$K_{MM}=\begin{cases} K_{MM}, & \text{if} \quad |q_M^{el}|\leq|q_{M,0}^{el}| \\ \gamma\delta K_{MM}\left(\frac{q_{M,0}^{el}}{q_M^{el}}\right)^{\delta+1}+\varepsilon^2 K_{NN}\left(1-\frac{q_{M,0}^{el}}{q_M^{el}}\right)^2, & \text{if} \quad |q_M^{el}|>|q_{M,0}^{el}| \end{cases} \tag{12}$$

This derivation is described in more detail in Chatzigogos et al. (2008), where a discussion concerning the assumption of constant K_{NN} is also provided.

Plasticity Model

For the definition of the plasticity model of the macroelement we examine the case of a footing resting on an elastoplastic soil obeying the classical Tresca criterion in which uplift at the soil-footing interface is not allowed.

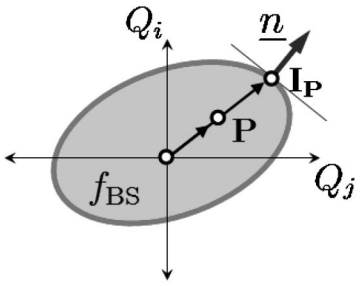

Fig. 3. Bounding surface and radial mapping rule for the definition of the image point

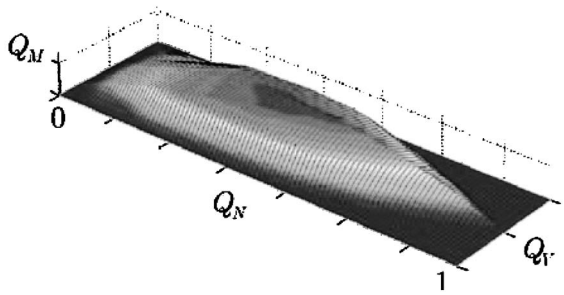

Fig. 4. Approximation from outside of the surface of ultimate loads of a circular footing on a homogeneous cohesive soil (cf. Chatzigogos et al., 2007). Uplift is allowed at the soil-footing interface

For this configuration we develop a ''bounding surface'' hypoplastic model following Dafalias and Hermann (1982) in order to describe plasticity developing in the system in a continuous way: a plastic response is obtained even for the first load increments (around the perimeter of the footing) and is continuously increasing with increasing external loading as we approach the bearing capacity of the system for which we obtain a situation corresponding to ''plastic flow''. The originality of the ''bounding surface'' hypoplasticity with respect to classical plasticity is the introduction of a f_{BS} surface in the space of generalized forces Q_i, called ***bounding surface*** allowing for a continuous and particularly flexible definition of the plastic modulus.

The role of this bounding surface in the present formulation is to define the cases of virgin loading/reloading and unloading loading in a way identical to classical plasticity and to define the direction of the plastic displacement increment and the magnitude of the plastic modulus. These two goals are achieved by introducing a mapping rule, which maps every point in the interior of the bounding surface to a specific point, called ***image-point***, on the surface boundary. The mapping adopted herein is a simple radial rule: for every point P at the interior of the bounding surface we define its corresponding image point $\mathbf{I}_P$ as follows (cf. Fig. 3):

$$\mathbf{I}_P = \{\lambda \mathbf{P} \,|\, \mathbf{I}_P \in \partial f_{BS} \text{ and } \lambda \geq 1\} \tag{13}$$

A Tresca medium gives commonly rise to an associated plasticity model at the scale of the soil and this feature has to be preserved in passing to the macroelement scale. For every point P in the interior of the boundary surface and if a loading force increment is considered, the direction of the plastic displacement increment follows the unit normal $\underline{n}$ on the bounding surface at the image point $\mathbf{I}_P$. Then the force increment is linked to the increment of plastic displacements with the equation:

$$\dot{\underline{Q}} = \underline{\underline{H}}\, \dot{\underline{q}}^{pl} \tag{14}$$

with the tensor $\underline{\underline{H}}$ defined as follows:

$$\underline{\underline{H}} = h\,(\underline{n} \otimes \underline{n}) \tag{15}$$

In Eq. (15), h is the plastic modulus. In the context of bounding surface hypoplasticity, h is usually defined as a function of some distance between the actual force state and its image point. As a measure of this distance we will use the positive scalar λ introduced in Eq. (13) and following Butterfield (1980), we will suppose a logarithmic reduction of the magnitude of plastic modulus as the stress point approaches the bounding surface:

$$h = h_0 \ln \lambda \tag{16}$$

A plastic response may be obtained during reloading as well (as it is the case for real soil behavior), if Eq. (16) is modified accordingly. A simple way to do this is to introduce the minimum value of the parameter λ during the loading history, denoted by λ_{min} and to write:

$$h = h_0 \ln \left[\left(\frac{\lambda}{\lambda_{min}} \right)^p \lambda \right], \tag{17}$$

In Eqs. (16), (17) h_0 and p are scalar numerical parameters to be calibrated from experimental data, typically a loading-unloading-reloading test of the footing under centered vertical load.

The meaning of Eqs. (16), (17) is clear: when λ is large, h is large and therefore the response is principally elastic. For small λ, h is small and the response is governed by the plastic displacements. In the case where the state of forces reaches the bounding surface $\lambda \to 1$, thus $h \to 0$ and the system is led to a state of plastic flow. For virgin loading $\lambda = \lambda_{min}$ and Eq. (16) is retrieved. In case of reloading $\lambda > \lambda_{min}$ and the plastic response is less pronounced than in the case of virgin loading, as it should be expected.

From the above remarks it is concluded that the bounding surface can be identified with the surface of ultimate loads of a circular footing on a homogeneous cohesive soil when uplift at the soil-footing interface ***is not allowed***. Randolph and Puzrin (2003) have produced optimal upper bounds for this surface which will be approximated herein by an ellipsoid centered at the origin. Its equation is of the form:

$$f_{BS}(\underline{Q}) = (Q_N)^2 + \left(\frac{Q_V}{Q_{V,\,max}} \right)^2 + \left(\frac{Q_M}{Q_{M,\,max}} \right)^2 = 1 \tag{18}$$

For a circular footing on a homogeneous cohesive soil we have: $Q_{V,\,max} = 1/6.06 = 0.165$ (sliding of the footing) and $Q_{M,\,max} \cong 0.67/6.06 = 0.11$ (cf. Randolph and Puzrin, 2003). The approximation of the bounding surface in the form of an ellipsoid, though particularly simplistic, is deemed to be sufficient for the present context of application. It is again emphasized, that the surface in Eq. (18) is

different from the surface of the ultimate loads of the system ***with uplift***, which has been determined (also by optimal upper bounds) in Chatzigogos et al. (2007) and is schematically presented in Fig. 4.

Uplift – Plasticity Coupling and Dynamic Loading

Uplift – plasticity coupling. In the previous paragraphs we examined each source of non-linearity separately. Here we give some comments concerning their coupling once they are both activated. An initial element of coupling between them is the definition of the moment of uplift initiation. Crémer et al. (2001, 2002) have shown through numerical analyses of strip footings that $Q_{M,0}$ is non-linear with respect to Q_N. They proposed the following fit:

$$Q_{M,0} = \pm \frac{Q_N}{\alpha} e^{-\zeta Q_N} \tag{19}$$

with the parameter ζ varying between 1.5 and 2.5.

In absence of specific numerical results for circular footings, a criterion for selecting the value of parameter ζ is that it should at least comply with the condition that all the states obtained with the macroelement lie within the surface of ultimate loads as it was explained in *Scope of the Model – Model Principles*. Indeed, in Chatzigogos et al. (2008) it is shown that the possible states of loading obtained from the presented plasticity and uplift models and $\zeta = 1.5 - 2.5$ are all included in the interior of the surface of ultimate loads of the system.

Except for the definition of uplift initiation, coupling between the two mechanisms is obtained without the introduction of additional parameters since they are both functions of the current force state: for example, an increment of imposed rotation will cause a change (through the plasticity model) in the value of Q_N, which will alter the parameters of the uplift model, etc. A detailed discussion on aspects of the uplift-plasticity coupling is given in Chatzigogos et al. (2008).

Dynamic loading. The domain of application of the presented model can be extended to dynamic loading by considering the following:

a. Identifying the parameters $\tilde{K}_{NN}$, $\tilde{K}_{VV}$, $\tilde{K}_{MM}$ in the uplift non-linear elastic model of the macroelement as the real part of the corresponding dynamic impedances of the footing.

b. Introducing the imaginary part of the retained dynamic impedances in order to account for the phenomenon of radiation damping. Table 2 presents commonly used approximate relationships for these quantities (cf. Gazetas, 1991). Off-diagonal terms are considered negligible. The expressions involve the Lysmer's analog velocity V_{La} given by the equation:

$$V_{La} = \frac{3.4}{\pi(1-\nu)} V_S \tag{20}$$

where V_S is the shear wave velocity of the soil.

c. The numerical treatment of the system is performed in the time domain and no dependence of the dynamic impedances on the frequency of excitation is considered. This problem can be partially remedied by considering dynamic impedances that correspond to some characteristic frequency of the system, (e.g., its fundamental eigen-frequency) or by using more sophisticated models for the impedances (cf. Saitoh, 2007).

d. Material damping in the soil is present in an area around the foundation where the soil enters into a plastic regime. This is directly reproduced by the plasticity model of the macroelement.

USING THE MACROELEMENT IN A PERFORMANCE-BASED DESIGN CONTEXT

As an application of the described macroelement model and aiming at demonstrating its utility in performance-based design, we are presenting a parametric study of the dynamic response of a specific structure subjected to a large number of real acceleration time histories. The objectives of the study are two-fold:

a) To examine the influence of the vertical component of the seismic input motion on the system response. This is motivated by the fact that residual settlements of the structure constitute an important criterion for evaluation of its overall performance and because both the plasticity and the uplift behavior of the structure are largely dependent on the levels of vertical force.

b) To investigate possible correlations between the displacements/rotation of the foundation (residual and extreme values) with severity parameters of the seismic input motion. This second objective aims at offering an insight onto those parameters of the seismic excitation that are more relevant in a performance/displacement-based context.

Examined Structure

Our study concerns a simplified representation of a pier of the Viaduc de l'Arc in France. The examined structure is shown in Fig. 5(a) and is modeled as presented in Fig. 5(b). The model exhibits four degrees of freedom: the horizontal translation of the Viaduc deck as well as the horizontal and vertical translations and the rotation of the foundation. The latter three will be described by the macroelement. Table 4 summarizes the adopted properties of the structural model. For the macroelement, we adopt the parameters described in the previous paragraphs for circular footings and a uplift-plasticity coupling parameter $\zeta = 1.5$. Using these quantities it is possible to form the mass, stiffness and damping matrices of the model and to calculate some important parameters for its description. These intermediate calculations are presented in Table 5.

The quantities in Table 4 reveal a soft soil deposit with a shear wave velocity $V_S = 200$ m/s and a relatively low safety factor of the foundation against static loads (FS = 1.75). The latter was chosen on purpose so that residual displacements of a certain magnitude are indeed induced, since it has been observed that the earthquake-induced residual displacements of shallow foundations are much more significant as the static safety factor is reduced, par-

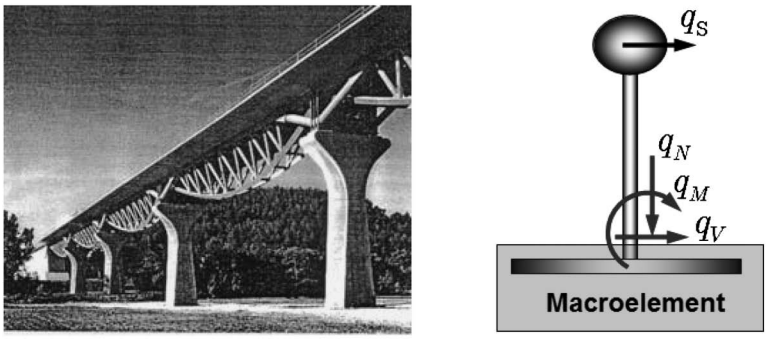

Fig. 5. (a) The columns of the Arc Viaduct in France (Design by Greisch Consultants) and (b) Simple model for dynamic analysis

Table 4. Properties of the considered structure

Property	Symbol	Units	Value
Mass of the superstructure	m_S	[kg]	1.500E+06
Mass of the foundation	m_F	[kg]	5.000E+05
Mass moment of inertia of the foundation	J_F	[kgm^2]	2.210E+07
Height of the superstructure	H	[m]	15.0
Diameter of the footing	D	[m]	12.0
Uniform soil cohesion	c	[Pa]	5.000E+04
Initial shear modulus of the soil	G	[Pa]	8.000E+07
Poisson's ratio of the soil	ν	[—]	0.5
Soil unit weight	γ	[N/m^3]	2.000E+04
Critical damping ratio of the superstructure	ξ_S	[%]	8.1
Stiffness of the superstructure	K_S	[N/m]	6.284E+08
Uplift – plasticity coupling parameter	ζ	[—]	1.5

ticularly for soft soil deposits (Mendoza and Auvinet, 1988). As a consequence, the response of the system will be mainly governed by the plasticity mechanism whereas uplift will be less important.

Finally, we note that for numerical application of the macroelement model and in absence of results for a specific real soil, the following representative values have been assigned to the parameters of the plasticity model: $h_0 = 0.1\,\bar{K}_{NN}$ and $p = 5$. In Chatzigogos et al. (2008) it is shown that these values perform good in predicting the response of a soft cohesive soil.

Selection of Acceleration Time Histories

The presented pier is subjected to a number of acceleration time histories recorded during real earthquakes. A total of twenty records have been considered. The time histories were obtained from the PEER and the NGA databases available on line at the link http://peer.berkeley.edu/nga/. In order for the selected time histories to be consistent with the considered soil profile, it was imposed that they have been recorded in a soil classified as deep broad soil (class D) or soft deep soil (class E) in the Geomatrix classification for the geotechnical subsurface characteristics (third letter of Geomatrix's classification, cf. NGA documentation at the link above) or have a preferred $V_{S,30} < 350$ m/s. Furthermore, the selected time histories were chosen so as to cover a large range of values for quantities such as the earthquake magnitude and distance, the peak ground acceleration, the duration of the strong motion, etc. Although no other strict selection criterion was imposed whatsoever, exceptionally severe acceleration records were not considered especially for the vertical component of the seismic input motion. In any case, the implemented macroelement model cannot reproduce total detachment/overturning or toppling of the structure so accelerograms leading to such situations were excluded.

For each record the PEER/NGA database provides three time histories corresponding to the vertical and the two horizontal components of the seismic excitation. Of these three, only the vertical component and one of the two horizontal components (usually the one with the largest PGA) were retained for the analyses. A number of quantities measuring the severity of each time history can be defined (cf. Nazé (2004) for an extensive list). In the present study the following quantities were examined (we use $a(t)$ for the recorded acceleration and d for the duration of the each record):

a. The Peak Ground Acceleration.

$$\mathrm{PGA} = \max_{0<t<d} \{|a(t)|\} \tag{21}$$

b. The maximum and minimum algebraic values of the ground velocity.

$$v^+ = \max_{0<t<d} \left\{ \int_0^t a(t)\mathrm{d}t \right\} \tag{22}$$

$$v^- = \min_{0<t<d} \left\{ \int_0^t a(t)\mathrm{d}t \right\} \tag{23}$$

c. The cumulative absolute velocity.

$$\mathrm{CAV} = \int_0^d |a(t)|\,\mathrm{d}t \tag{24}$$

d. The Arias Intenstiy.

Table 5. Parameters of the considered structural model determined by intermediate calculations

Property	Symbol	Units	Value	Comments
Shear wave velocity of the soil	V_S	[m/s]	200.00	$V_S = \sqrt{\frac{G}{\rho}},\ \rho = \frac{\gamma}{g}$
Lysmer's analog velocity	V_{La}	[m/s]	432.90	Equation (20)
Vertical stiffness of the foundation	$\tilde{K}_{NN}$	[N/m]	3.840E + 09	From Table 2
Horizontal stiffness of the foundation	$\tilde{K}_{VV}$	[N/m]	2.560E + 09	From Table 2
Rotational stiffness of the foundation	$\tilde{K}_{MM}$	[Nm/rad]	9.216E + 10	From Table 2
Imaginary part of the dynamic impedance in the vertical direction	C_{NN}	[Ns/m]	9.792E + 07	From Table 2
Imaginary part of the dynamic impedance in the horizontal direction	C_{VV}	[Ns/m]	4.524E + 07	From Table 2
Imaginary part of the dynamic impedance in the rotational DOF	C_{MM}	[Nms/rad]	8.813E + 08	From Table 2
Damping parameter of the superstructure	C_S	[Ns/m]	4.963E + 06	$C_S = 2\xi_S\sqrt{m_S K_S}$
Critical damping ratio of the structure + foundation in the vertical direction	ξ_N	[%]	55.9	$\xi_N = \frac{C_{NN}}{2\sqrt{(m_S + m_F)\tilde{K}_{NN}}}$
Total weight of the structure (superstructure + foundation)	W_{tot}	[N]	1.962E + 07	$W_{tot} = (m_S + m_F)\, g$
Maximum vertical force supported by the foundation	N_{max}	[N]	3.427E + 07	$N_{max} = 6.06c\frac{\pi D^2}{4}$
Static factor of safety of the foundation	FS	[—]	1.747	$FS = \frac{W_{tot}}{N_{max}}$

Table 6. Accererogram records considered in the parametric analysis

N/N	NGA/PEER Database Number	Earthquake	GEOMATRIX Classification	Preferred $V_{S,30}$	Joyner-Boore Distance	Epicentral Distance	Moment Magnitude
				[m/s]	[km]	[km]	
1	N0130	Friuli	C	338.60	10.99	17.12	5.91
2	P0807	Cape Mondecino	D	338.50	40.23	53.34	7.01
3	N1631	Upland	D	229.80	0.00	10.82	5.63
4	N0564	Kalamata	C	338.60	0.00	9.97	6.20
5	N1147	Kocaeli	E	175.00	68.09	112.26	7.51
6	N0096	Managua	D	288.00	0.00	5.68	5.20
7	P0548	Chalfant Valley	D	271.40	6.07	10.54	5.77
8	P0233	Mamoth Valley	D	370.80	4.48	10.91	6.06
9	P0148	Coyote Lake	D	270.00	8.47	10.94	5.74
10	P1540	Duzce	D	276.00	0.00	1.61	7.14
11	N0721	Superstition Hills	D	192.10	18.20	35.30	6.54
12	P0368	Coalinga	D	257.40	7.69	9.98	6.36
13	N1853	Yountville	D	271.40	0.00	9.89	5.00
14	N0692	Whittier Narrows	D	308.60	11.47	11.73	5.99
15	P1182	Chi-Chi	D	258.90	9.96	31.96	7.62
16	P0802	Erzincan	D	274.50	0.00	8.97	6.69
17	P0927	Northridge	D	269.10	3.16	20.27	6.69
18	P0530	Palm Springs	D	345.00	0.00	10.57	6.06
19	P0161	Imperial Valley	D	223.00	0.47	6.20	6.53
20	P1024	Northridge	D	370.50	0.00	13.60	6.69

Table 7. Severity parameters of horizontal and vertical components of the considered records

N/N	Earthquake	d	HORIZONTAL COMPONENT					VERTICAL COMPONENT		
			PGA	v^+	v^-	CAV	I_A	PGA	CAV	I_A
		[s]	[g]	[m/s]	[m/s]	[m/s]	[cm/s]	[g]	[m/s]	[cm/s]
1	Friuli	26.39	0.110	0.08	−0.10	2.68	14.25	0.074	1.285	3.45
2	Cape Mondecino	44.00	0.154	0.20	−0.14	5.57	30.30	0.042	3.184	7.37
3	Upland	40.00	0.186	0.08	−0.11	3.45	26.45	0.097	2.050	7.92
4	Kalamata	29.24	0.248	0.29	−0.24	4.41	54.99	0.204	3.425	30.96
5	Kocaeli	150.41	0.249	0.40	−0.33	14.53	100.62	0.079	5.761	13.81
6	Managua	19.99	0.271	0.19	−0.34	4.54	50.76	0.200	2.672	20.79
7	Chalfant Valley	39.87	0.285	0.17	−0.17	5.38	52.66	0.205	3.399	20.52
8	Mamoth Valley	29.96	0.311	0.16	−0.11	5.91	67.77	0.203	5.550	53.23
9	Coyote Lake	26.86	0.339	0.25	−0.16	3.99	51.26	0.166	2.806	22.17
10	Duzce	25.89	0.348	0.54	−0.60	13.60	269.46	0.357	8.249	113.25
11	Superstition Hills	40.00	0.358	0.46	−0.17	9.50	106.25	0.128	4.560	21.16
12	Coalinga	39.96	0.380	0.32	−0.31	9.58	157.05	0.206	7.211	69.89
13	Yountville	72.00	0.409	0.20	−0.40	5.79	109.24	0.513	3.588	46.95
14	Whittier Narrows	37.84	0.426	0.38	−0.30	6.87	123.56	0.206	4.077	35.97
15	Chi-Chi	90.00	0.440	1.15	−0.90	21.19	239.79	0.165	9.102	52.01
16	Erzincan	20.78	0.515	0.84	−0.53	7.54	150.38	0.248	5.134	50.16
17	Northridge	40.00	0.583	0.56	−0.75	14.38	424.95	0.548	11.430	265.24
18	Palm Springs	20.03	0.694	0.19	−0.34	7.01	157.25	0.435	5.991	97.86
19	Imperial Valley	37.61	0.775	0.46	−0.38	17.79	598.73	0.425	8.126	112.30
20	Northridge	40.00	0.828	0.43	−1.17	14.66	449.58	0.377	8.854	156.06

$$I_A = \frac{\pi}{2g}\int_0^d a^2(t)\mathrm{d}t \tag{25}$$

It is clear from the definitions of the above quantities that PGA, v^+ and v^- exhibit an ***instantaneous*** character expressing an extreme value of the ground acceleration or velocity. On the other hand, parameters such as CAV and I_A are ***cumulative***, in the sense that they are expressed as a temporal integration of some quantity throughout the time history. It is noted that the value of the duration d is calculated directly from the record as the number of data points times the time increment. Since d by itself will not be used for correlations there is no reason to use a more precise definition of it.

Table 6 provides a list of the records considered in the analysis. The preferred $V_{S,30}$ varies for all records from 175 m/s to 370 m/s, which is consistent with the selected soil profile. The same table also provides the Joyner-Boore and epicentral distance and the moment magnitude of each record. The severity parameters introduced in Eqs. (21)–(25) are presented in Table 7. These values will be used to investigate possible correlations with the response of the system. It is seen that for the considered records, the vertical component of the seismic input motion presents a certain regularity with respect to the horizontal one. PGA values range from 0.11 g up to 0.83 g for the horizontal component and from 0.04 g up to 0.55 g for the vertical component. For the records N°10 and N°13 the PGA of the vertical component is larger than the PGA of the horizontal one.

Performed Analyses

Using the two time histories (horizontal – vertical component) that are retained from each record, three separate non-linear dynamic analyses of the structure are performed: a) under the horizontal component alone, b) under the vertical component alone and c) under the horizontal and vertical components acting simultaneously. The structure is always subjected to the combination of the horizontal and vertical components that come from the same record.

For each analysis we calculate the complete time histories of all the forces and displacements in the model. Among them, we keep track of the following quantities:

a. The residual settlement of the foundation $u_z(d)$.
b. The residual rotation of the foundation $\theta_y(d)$.
c. The residual horizontal displacement $u_x(d)$.
d. The maximum and minimum algebraic values of the footing rotations:

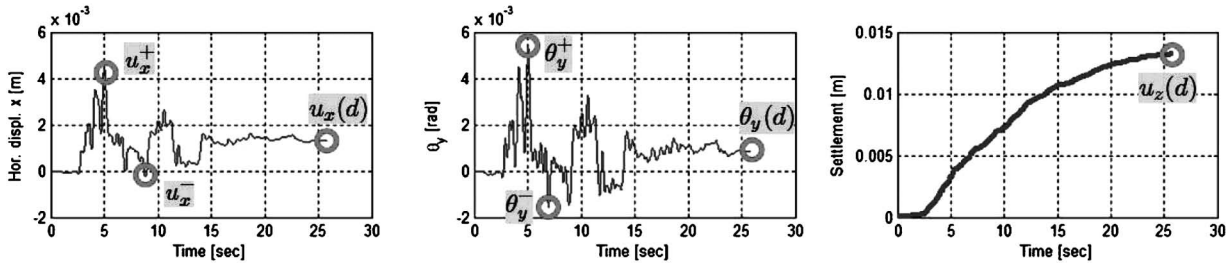

Fig. 6. Characteristic displacements and rotations recorded for each non-linear dynamic analysis

Table 8. Classification of characteristic elements of the response of the considered system

Quantity	Under Horizontal Compontent only	Under Vertical Component only	Under the combination of both components
Residual settlement $u_z(d)$	Quasi-monotone Cumulative	Quasi-monotone Cumulative	Quasi-monotone Cumulative
Residual rotation $\theta_y(d)$	Non-monotone Cumulative	—	Non-monotone Cumulative
Extreme values of rotation θ_y^+, θ_y^-	Instantaneous	—	Instantaneous
Residual horizontal displacement $u_x(d)$	Non-monotone Cumulative	—	Non-monotone Cumulative
Extreme values of horizontal displacement u_x^+, u_x^-	Instantaneous	—	Instantaneous
Dissipated Energy in the system ε_d	Monotone Cumulative	Monotone Cumulative	Monotone Cumulative

$$\theta_y^+ = \max_{0<t<d} \{\theta_y(t)\} \tag{26}$$

$$\theta_y^- = \min_{0<t<d} \{\theta_y(t)\} \tag{27}$$

e. The maximum and minimum algebraic values of the footing horizontal displacements:

$$u_x^+ = \max_{0<t<d} \{u_x(t)\} \tag{28}$$

$$u_x^- = \min_{0<t<d} \{u_x(t)\} \tag{29}$$

f. The dissipated energy in the system ε_d.

The dissipated energy ε_d is entirely concentrated in the foundation and is calculated as follows:

$$\varepsilon_d = N_{max} D \left(\int_0^d \underline{Q} \cdot \underline{\dot{q}}^{pl} \, dt \right) \tag{30}$$

Figure 6 presents a typical calculation of the horizontal displacement, rotation and settlement time histories of the center of the footing obtained from an analysis under the horizontal component alone, in which the quantities (a)–(e) are identified.

The above quantities are classified in Table 8 with respect to: a) whether they are ***instantaneous*** or ***cumulative*** (in the same sense as the parameters describing the severity of the seismic input motion) and b) in case they are cumulative, whether they are ***monotonically*** varying or not. For example, ε_d is (by definition) cumulative and monotonically increasing. Similarly, the residual settlement of the foundation is cumulative throughout the time history and may be classified as ***quasi-monotonically*** varying in all three cases of analysis. This is verified by examination of the typical evolution of the footing settlement presented in Fig. 6. It is not strictly monotonic because primarily there is a possibility that the footing is detached from the soil to such an extent that uplift of the footing center occurs. For the examined structure, this possibility is small because the response of the system is mainly governed by the plasticity mechanism (cf. *Examined Structure*). A second reason is that when the vertical load is diminished there is a very small yet present elastic rebound which is taken into account in the model through the term $\tilde{K}_{NN}$ of the elastic stiffness matrix. Due to the quasi-monotonicity of this quantity, the maximum settlement of the structure during the excitation is readily identified with its residual settlement $u_z(d)$. The quantities $\theta_y(d)$, $u_x(d)$ can also be qualified as cumulative, since they are obtained at the end of the excitation. However, they are ***non-monotonically*** varying since they can equally be accumulated in both directions. Finally, the quantities θ_y^+, θ_y^-, u_x^+, and u_x^- are instantaneous. The scope of this classification is clear: it is expected that cumulative displacements will be correlated to cumulative severity parameters (CAV, I_A), whereas instantaneous characteristic displacements with severity parameters such as the PGA, v^+ and v^-.

Results

The results are presented in Table 9 for the analyses with the horizontal component alone and in Table 10 for the analyses with the vertical component alone and the two components together. They are discussed in the following paragraphs.

Residual Settlements and Dissipated Energy

Influence of the vertical component. The residual settlements of the foundation for the 20 seismic scenarios and the three types of analyses that have been performed

Table 9. Results of the analyses with the horizontal component acting alone (H)

N/N	Earthquake	H							
		$u_z(d)$	$\theta_y(d)$	θ_y^+	θ_y^-	$u_x(d)$	u_x^+	u_x^-	ε_d
		[m]	[rad]	[rad]	[rad]	[m]	[m]	[m]	[Nm]
1	Friuli	0.0047	−2.652E−05	7.871E−04	−5.125E−04	8.858E−05	4.129E−04	−1.590E−04	1.222E+06
2	Cape Mondecino	0.0090	9.709E−05	5.017E−04	−9.121E−04	7.951E−05	2.419E−04	−5.142E−04	2.260E+06
3	Upland	0.0054	7.775E−05	5.244E−04	−4.894E−04	2.594E−04	4.719E−04	−1.849E−04	1.337E+06
4	Kalamata	0.0057	1.175E−03	1.789E−03	−1.828E−03	9.038E−04	1.210E−03	−1.151E−03	1.639E+06
5	Kocaeli	0.0225	−1.669E−03	1.689E−03	−2.825E−03	−8.805E−04	1.213E−03	−1.397E−03	6.156E+06
6	Managua	0.0060	−2.599E−04	2.041E−03	−8.704E−04	1.172E−04	1.464E−03	−5.043E−04	1.621E+06
7	Chalfant Valley	0.0083	8.702E−06	6.492E−04	−1.116E−03	−7.970E−05	3.466E−04	−6.142E−04	2.139E+06
8	Mamoth Valley	0.0082	−1.669E−04	3.832E−04	−7.281E−04	−2.346E−04	2.330E−04	−5.229E−04	2.022E+06
9	Coyote Lake	0.0058	1.570E−03	2.445E−03	−1.230E−03	1.497E−03	1.948E−03	−8.014E−04	1.617E+06
10	Duzce	0.0132	8.469E−04	5.334E−03	−1.559E−03	1.324E−03	4.381E−03	−2.290E−04	4.526E+06
11	Superstition Hills	0.0118	3.227E−03	4.329E−03	−1.670E−03	2.975E−03	3.422E−03	−5.529E−04	3.263E+06
12	Coalinga	0.0128	1.179E−04	2.437E−03	−1.763E−03	3.777E−04	1.905E−03	−9.047E−04	3.913E+06
13	Yountville	0.0080	1.201E−03	3.343E−03	−1.548E−03	1.132E−03	2.201E−03	−9.764E−04	2.424E+06
14	Whittier Narrows	0.0084	−6.638E−04	1.658E−03	−2.811E−03	−7.437E−04	1.030E−03	−1.835E−03	2.422E+06
15	Chi-Chi	0.0257	−8.617E−03	4.300E−03	−1.461E−02	−7.852E−03	2.400E−03	−1.171E−02	8.555E+06
16	Erzincan	0.0094	−9.275E−03	2.119E−03	−1.526E−02	−9.860E−03	1.187E−03	−1.291E−02	3.803E+06
17	Northridge	0.0144	−2.876E−03	2.877E−03	−6.649E−03	−3.812E−03	8.450E−04	−5.964E−03	5.120E+06
18	Palm Springs	0.0087	1.353E−03	2.402E−03	−8.805E−04	5.634E−04	1.358E−03	−5.386E−04	2.418E+06
19	Imperial Valley	0.0143	−3.630E−03	6.548E−03	−5.340E−03	5.009E−05	6.810E−03	−1.303E−03	5.754E+06
20	Northridge	0.0169	1.070E−02	1.579E−02	−6.613E−04	8.145E−03	1.205E−02	−3.975E−04	6.677E+06

are presented in Fig. 7. As it is revealed from the diagram, the residual settlements obtained when the vertical component acts alone are the largest ones, reaching a maximum value of approximately 14 cm. On the contrary, the residual settlements for the analyses with the horizontal component alone are an order of magnitude smaller and do not exceed the value of 2.5 cm. The residual settlement obtained for the combination of the two components lies systematically between the two previous values:

$$u_z(d)_V > u_z(d)_{H+V} > u_z(d)_H \tag{31}$$

If the residual settlement of the footing is considered as the performance indicator of the structure, Eq. (31) shows that consideration of the horizontal component alone is non-conservative whereas consideration of the vertical component alone is conservative.

The same remark holds for the dissipated energy at the foundation. The results of the seismic scenarios and the three types of analyses are presented in Fig. 8 and they lead to the same conclusion:

$$\varepsilon_{d,V} > \varepsilon_{d,H+V} > \varepsilon_{d,H} \tag{32}$$

It is concluded from these observations that as the two components act together, the horizontal component ''steals'' so to speak some of the action of the vertical one, leading to a less severe response. The effect of the horizontal component can be understood if it is noticed that the vertical acceleration imposed on the structure oscillates much faster than the horizontal one. With this observation in mind, let us examine typical stress paths in the space of the generalized forces in the plane Q_N-Q_V. These are schematically represented in Fig. 9. When the horizontal component acts alone, the force path will start at some point on the axis of Q_N (weight of the structure) and it will oscillate in a direction parallel to the axis of horizontal forces Q_V. Similarly, for the analysis with the vertical component alone, an oscillating force path will be obtained ***along*** the axis Q_N. If during this type of excitation we consider a loading force increment $\dot{\underline{Q}}_N$, then we can argue that the increment of dissipated energy in the system:

$$\dot{\varepsilon}_{d,N} = \frac{1}{h}(\dot{\underline{Q}}_N \cdot \underline{n}_N)^2 \tag{33}$$

is maximized since $\dot{\underline{Q}}_N$ is aligned with the direction of plastic displacements. This direction is defined by the unit normal vector $\underline{n}_N$ at the corresponding image point on the bounding surface also represented in the figure. We next consider the case of the two components (horizontal and

Table 10. Results of the analyses with the vertical component alone (V) and the two components acting together (H + V)

N/N	Earthquake	V		H + V							
		$u_z(d)$	ε_d	$u_z(d)$	$\theta_y(d)$	θ_y^+	θ_y^-	$u_x(d)$	u_x^+	u_x^-	ε_d
		[m]	[Nm]	[m]	[rad]	[rad]	[rad]	[m]	[m]	[m]	[Nm]
1	Friuli	0.0180	4.192E+06	0.0108	−2.162E−04	7.110E−04	−6.265E−04	−2.483E−04	3.919E−04	−5.108E−04	2.634E+06
2	Cape Mondecino	0.0170	3.997E+06	0.0157	1.906E−04	5.538E−04	−8.938E−04	9.766E−05	2.235E−04	−5.711E−04	3.841E+06
3	Upland	0.0309	7.169E+06	0.0243	−2.981E−06	5.613E−04	−4.296E−04	5.782E−04	9.816E−04	−3.319E−04	5.722E+06
4	Kalamata	0.0437	9.964E+06	0.0250	2.346E−03	2.897E−03	−4.968E−04	2.543E−03	3.003E−03	−4.927E−04	6.042E+06
5	Kocaeli	0.0568	1.330E+07	0.0443	−1.960E−03	1.363E−03	−3.080E−03	−5.078E−04	1.191E−03	−1.257E−03	1.125E+07
6	Managua	0.0400	9.219E+06	0.0201	−1.256E−03	1.601E−03	−1.872E−03	−8.806E−04	1.279E−03	−1.582E−03	4.923E+06
7	Chalfant Valley	0.0534	1.226E+07	0.0357	8.773E−04	1.165E−03	−8.041E−04	3.970E−04	9.406E−04	−4.053E−04	8.455E+06
8	Mamoth Valley	0.0902	2.058E+07	0.0766	−1.641E−04	8.188E−04	−6.625E−04	1.808E−03	2.094E−03	−2.575E−04	1.773E+07
9	Coyote Lake	0.0442	1.008E+07	0.0331	1.302E−03	2.348E−03	−1.194E−03	5.857E−04	9.911E−04	−1.391E−03	7.814E+06
10	Duzce	0.1306	2.929E+07	0.0653	7.051E−03	9.599E−03	−2.025E−03	2.470E−03	4.639E−03	−2.215E−03	1.627E+07
11	Superstition Hills	0.0638	1.478E+07	0.0355	2.566E−03	4.202E−03	−1.749E−03	2.105E−03	3.019E−03	−9.832E−04	8.824E+06
12	Coalinga	0.0705	1.637E+07	0.0375	4.183E−04	2.792E−03	−1.364E−03	−2.640E−04	1.834E−03	−8.471E−04	9.538E+06
13	Yountville	0.0403	9.097E+06	0.0319	1.686E−03	3.674E−03	−7.880E−04	9.702E−04	1.943E−03	−1.384E−03	7.757E+06
14	Whittier Narrows	0.0672	1.538E+07	0.0478	−1.985E−03	1.303E−03	−3.273E−03	−7.316E−04	1.179E−03	−1.793E−03	1.149E+07
15	Chi-Chi	0.1036	2.398E+07	0.0478	−8.326E−03	4.795E−03	−1.387E−02	−8.380E−03	2.197E−03	−1.211E−02	1.376E+07
16	Erzincan	0.0642	1.475E+07	0.0305	−8.721E−03	3.439E−03	−1.384E−02	−8.971E−03	2.598E−03	−1.170E−02	8.708E+06
17	Northridge	0.1317	3.038E+07	0.0737	−2.203E−03	4.103E−03	−6.210E−03	−3.521E−03	3.046E−03	−4.698E−03	1.903E+07
18	Palm Springs	0.0905	2.016E+07	0.0674	2.727E−04	1.638E−03	−1.215E−03	3.348E−04	1.689E−03	−1.292E−03	1.550E+07
19	Imperial Valley	0.1416	3.153E+07	0.0765	−1.160E−02	1.860E−03	−1.351E−02	1.017E−03	4.090E−03	−2.539E−03	1.947E+07
20	Northridge	0.1339	2.946E+07	0.0690	1.021E−02	1.506E−02	−2.896E−03	4.313E−03	9.122E−03	−3.542E−03	1.844E+07

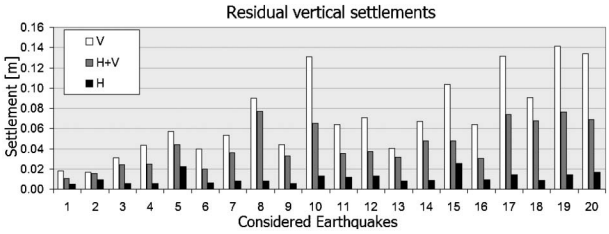

Fig. 7. Residual settlements of the foundation for the considered records and for the three cases of analyses

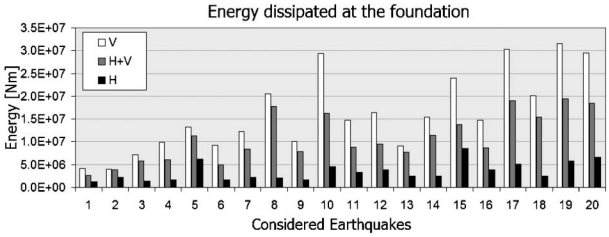

Fig. 8. Total dissipated energy at the foundation for the considered records and for the three cases of analyses

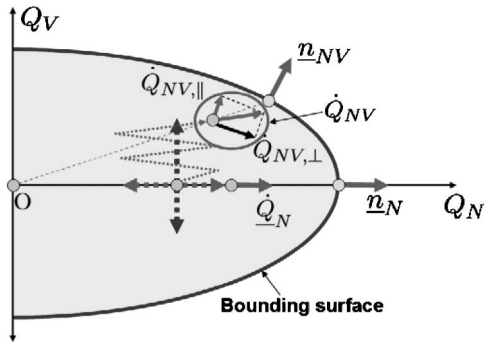

Fig. 9. Schematic representation of typical stress paths in the space of the generalized forces (plane Q_N-Q_V)

vertical) acting simultaneously. Since the frequency content of the vertical motion oscillates much faster than horizontal one, we will have: $\dot{\underline{Q}}_{NV} \approx \dot{\underline{Q}}_N$. However, the presence of the horizontal motion will move the current force state away from axis Q_N and will have thus changed the direction of the increment of plastic displacements defined on the corresponding image point on the bounding surface. Denoting this new direction as $\underline{n}_{NV}$ it is clear that the increment $\dot{\underline{Q}}_{NV}$ can be decomposed into a component

$\dot{\underline{Q}}_{\mathrm{NV},\perp}$ perpendicular to $\underline{n}_{\mathrm{NV}}$ and a component $\dot{\underline{Q}}_{\mathrm{NV},\parallel}$ parallel to $\underline{n}_{\mathrm{NV}}$. The response of the system under $\dot{\underline{Q}}_{\mathrm{NV},\perp}$ is purely elastic (cf. Fig. 9), and the increment of dissipated energy in the system is:

$$\dot{\varepsilon}_{\mathrm{d,\,NV}} = \frac{1}{h}(\dot{\underline{Q}}_{\mathrm{NV}} \cdot \underline{n}_{\mathrm{NV}})^2 \approx \frac{1}{h}(\dot{\underline{Q}}_{\mathrm{N}} \cdot \underline{n}_{\mathrm{NV}})^2 < \frac{1}{h}(\dot{\underline{Q}}_{\mathrm{N}} \cdot \underline{n}_{\mathrm{N}})^2 = \dot{\varepsilon}_{\mathrm{d,\,N}} \tag{34}$$

In the above reasoning, it has been implied that h is the same for the two loading scenarios. Actually, η (although it might be smaller in the NV case) remains comparable for the two scenarios during the largest part of the loading history. Therefore, it does not alter the validity of the presented argument.

Eqs. (31) and (32) should not be regarded as completely general results. They hold in the framework of the adopted plasticity model since the considered vertical components are of some comparable intensity with respect to the horizontal ones and also because plasticity is the governing mechanism of the response: the foundation oscillates up and down or back and forth pushing the ground downwards. They reveal however the undisputed usefulness of macroelement modeling in investigating subtle features of non-linear dynamic response.

Correlations with severity parameters. The objective of this paragraph is to investigate the severity parameters of the seismic input motion which best correlate with the obtained results. Our main interest is in the residual settlement of the foundation since it is a quantity that may be used as a performance indicator for the structure. On the contrary, the dissipated energy at the foundation is less important since it cannot easily be correlated to the performance of the structure. From the obtained results and the values presented in Table 7 it can be shown that the residual settlements of the foundation correlate very satisfactorily with the cumulative absolute velocity of the imposed acceleration histories. Figure 10 plots the residual settlements versus CAV for the three types of performed analyses. In the case of the horizontal and vertical components acting alone the correlation is very satisfactory with a R^2 in the order of 0.82–0.83. For the case of the two components acting together, the correlation is not as good, primarily because it is not clear how CAV should be defined in this case. In Fig. 10, the mean of the two CAVs is considered in order to emphasize that the obtained result is between the values for the components acting alone. Other possible definitions for the mixed CAV may be proposed such as integrating the Euclidean measure of the two components, etc.

We note finally that the correlation of the residual settlements with the Arias intensity is significantly worse than the one achieved with the CAV. This observation shows that the duration of the record and the magnitude of the induced accelerations are both important for determining the final response. In Arias intensity, a priority is given to the magnitude of the induced accelerations since it is the acceleration squared that is being integrated all through the time history. Again, this feature may be attributed to the soil being soft and the plasticity model predicting cycle stabilization in repeated loading. Consequently, significant displacements are also obtained in reloading, i.e., after the largest earthquake shock.

Rotations and Horizontal Displacements

Influence of the vertical component. The residual and extreme rotations of the foundation for the 20 seismic scenarios and the two types of analyses (analyses with the vertical component alone are of no interest in this case) are presented respectively in Figs. 11 and 12. The residual rotation reaches up to 0.01 rad $\approx 0.5°$ and the extreme rotation about 1.5 times more. The residual horizontal displacements reach up to approximately 1 cm so they are considerably smaller than the settlements of the footing. The following remarks can be done:

i. The presence of the vertical component does not seem to alter significantly the values of the residual, extreme rotations and horizontal displacements of the foundation. The influence is less important on the horizontal displacements. There does not seem to be a general rule as to whether the vertical component increases or reduces the response.

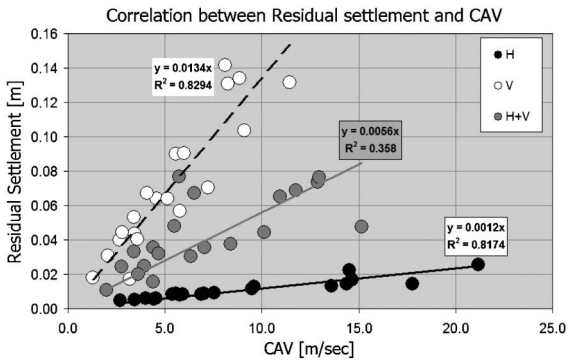

Fig. 10. Correlation between CAV and residual settlements of the foundation

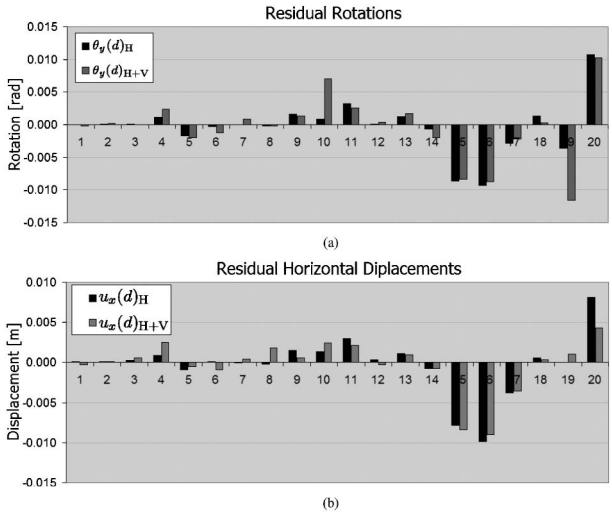

Fig. 11. (a) Residual rotations and (b) Residual horizontal displacements of the foundation

ii. Regarding the rotations of the foundation there are certain cases (for example, N°10 and N°19) where the vertical component has a significant effect on the response while the same is not observed for the horizontal displacements. This can be attributed to the uplift mechanism that affects uniquely the moment-rotation relationship. It is recalled that uplift may be present even if the footing center settles since the uplift mechanism is coupled with the plasticity one.

iii. In Fig. 13, the residual and extreme rotations of the foundation are plotted versus the corresponding horizontal displacements for the analyses with the horizontal component alone and with the two components acting together. In the first case (cf. Fig. 13(a)), the correlation is very satisfactory; it stems from the oscillation of the single-degree-of-freedom superstructure. When the vertical component is also considered (cf. Fig. 13(b)), a satisfactory correlation is also obtained which is however not as good as before because the amplified uplift effect increases the rotation uniquely without affecting the horizontal displacement (cf. seismic scenario N°19).

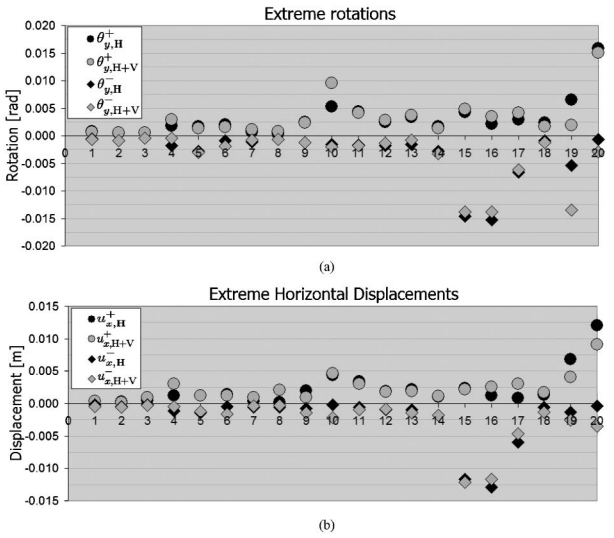

Fig. 12. (a) Extreme values of rotations and (b) Extreme values of horizontal displacements of the foundation

Correlations with severity parameters. Trying to find severity parameters that correlate with the characteristic rotations or horizontal displacements of the foundation is much more difficult than in the case of settlements because of the non-monotonic variation and instantaneous character of the former. Notwithstanding the uncertainties related to such an effort we can observe the following:

i. The values $\theta_y(d)$ and $u_x(d)$ seem to be correlated with the sums $1/2(\theta_y^+ + \theta_y^-)$ and $1/2(u_x^+ + u_x^-)$ respectively. A physical interpretation of this is that the structure oscillates between the position of the maximum and minimum algebraic rotation θ_y^+ and θ_y^- (same for u_x^+ and u_x^-). If one is larger than the other in absolute value, then an eccentricity is created in the corresponding direction and a residual rotation appears with the same sign as the aforementioned sums. The results are presented in Fig. 14 and show a satisfactory correlation although there are some cases that deviate from the trend. It is interesting to point out that the residual values are larger than the corresponding sums of extreme values: there seems to be a build up of residual rotation/displacement once an eccentricity has been created towards a particular direction.

ii. As far as the extreme values are concerned and due to their instantaneous character, it is expected that they correlate with some instantaneous severity parameter. The proposed parameters are v^+ and v^- (cf. Eqs. (22), (23)). The correlation is presented in Fig. 15: it is proved quite satisfactory especially for the rotations.

iii. A direct correlation of the residual values of rotations and displacements with a severity parameter of the seismic input motion seems unrealistic due to the multitude of factors that may influence the result. At this point, only the ''eccentricity'' of the seismic motion could be roughly anticipated by examining the quantity

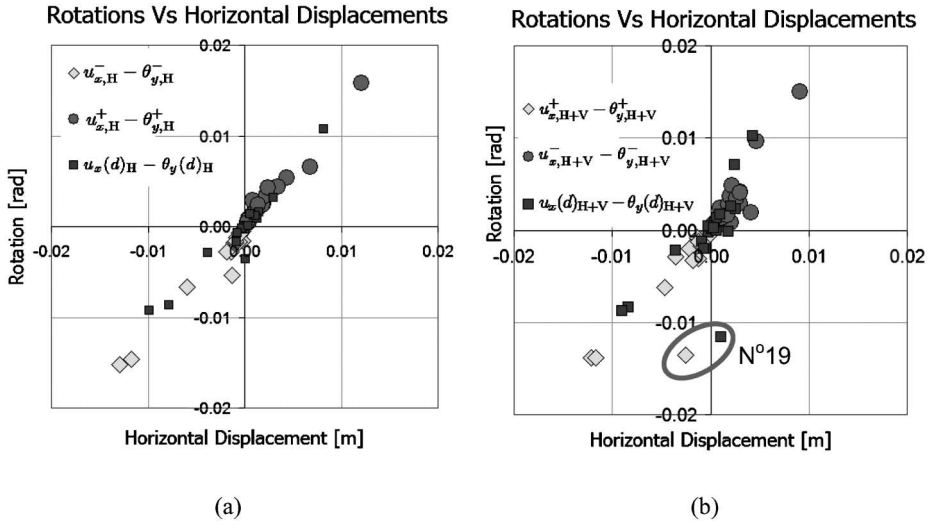

Fig. 13. Characteristic rotations of the foundation plotted versus the corresponding horizontal displacements: (a) Analyses H and (b) Analyses H + V

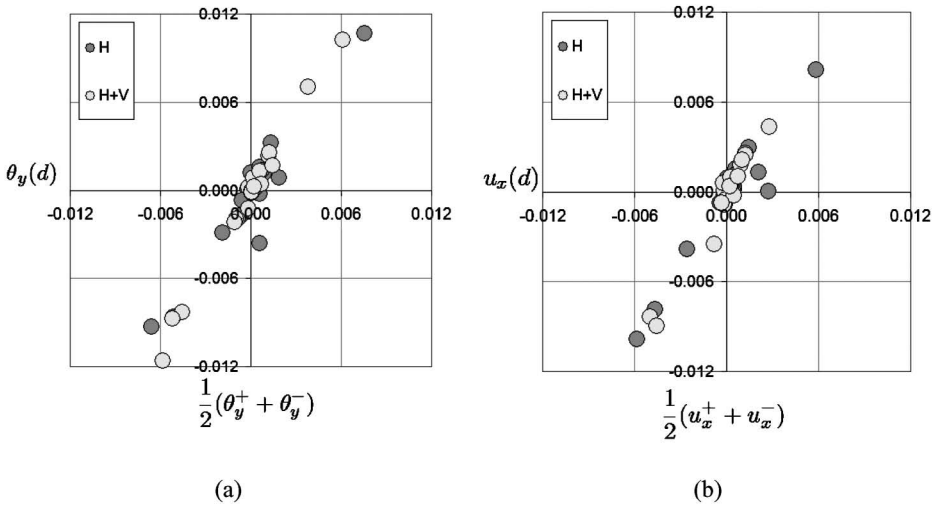

Fig. 14. Correlations between difference of extreme values versus residual values for (a) rotation and (b) horizontal displacements of the foundation

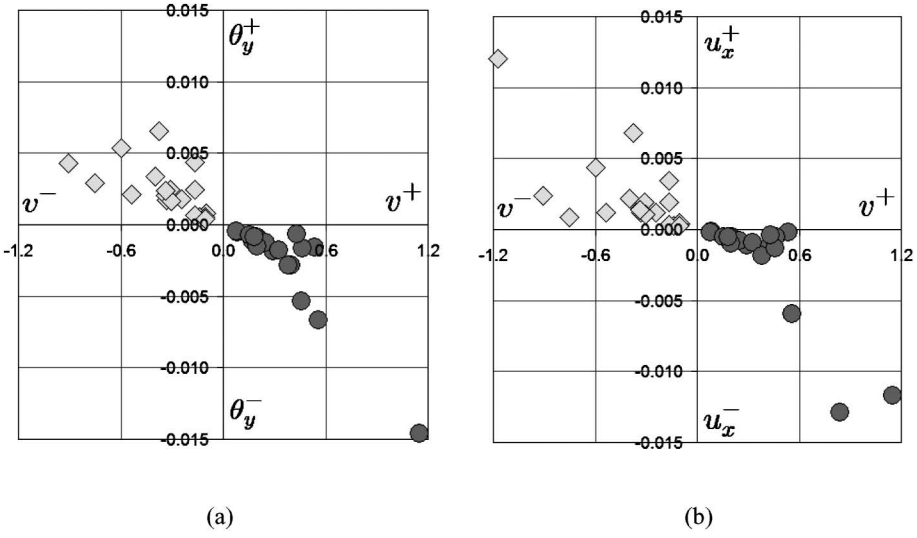

Fig. 15. Correlations between v^+, v^- and extreme values of (a) rotations and (b) horizontal displacements

$(v^+ + v^-)$, notwithstanding the large complexity of the examined phenomenon.

CONCLUSIONS

We have presented in this paper a parametric analysis of the non-linear dynamic response of a bridge pier founded on a soft cohesive soil when subjected to a real earthquake. A total of sixty non-linear dynamic analyses were presented in which the soil-foundation system was replaced by an original macroelement attached at the base of the pier and reproducing the material and geometric non-linearities taking place at the soil-footing interface. The performed analyses demonstrated the versatility and usefulness of macroelement modeling of foundations in performing efficiently a large number of non-linear dynamic soil-structure interaction analyses dedicated to performance-based design applications. We may emphasize the following points:

i. The macroelement model was very successful in capturing the qualitative aspects of the response: the soft soil conditions and the low static safety factor of the foundation gave rise to a response governed by the plasticity mechanism whereas uplift was less significant. The model predicted significantly larger settlements than horizontal displacements or rotations which is in perfect agreement with seismic failure observed in similar conditions (cf. Mendoza and Auvinet, 1988)

ii. It was possible to investigate the effect of the vertical component of the seismic input motion and to reveal its crucial role especially with respect to the residual settlement of the foundation. Subtle features of the response were explained based on the adopted model characteristics.

iii. The results of the analyses were used to establish correlations between parameters of the system response

and parameters describing the severity of the seismic input motion. It was shown that response parameters of cumulative or instantaneous nature correlate with severity parameters of the same nature. Very satisfactory correlations were established between the residual settlements of the footing with the cumulative absolute velocity of the accelerograms. The extreme rotations and horizontal displacements were shown to be correlated with parameters such as v^+ and v^-. The "eccentricity" of the response was correlated with the sum $(v^+ + v^-)$. Moreover, it was possible to explain why certain cases seemed to deviate from the observed trends (e.g., presence of significant uplift, etc).

iv. In the present study we studied the excitation – response relationship of a particular structure. Clearly the macroelement can be used for other types of parametric analyses. In terms of modeling, the presented macroelement model remains very flexible and extensible in the sense that several aspects of the system behavior can be easily integrated in it: three-dimensional loading, soil friction and non-associated plastic flow, frequency-dependent foundation impedances (simplified models), P-δ effects, reduction of the footing bearing capacity because of the presence of inertial forces in the ground, etc.

The presented results have revealed that the concept of macroelement can and will serve as a powerful tool towards the promising philosophy of performance-based design.

ACKNOWLEDGMENTS

This work has been performed during the post-doctoral stage of the first author at the Laboratoire de Matériaux et de Structures du Génie Civil (France). The Ecole Polytechnique (Palaiseau, France) and the Ecole Nationale des Ponts et Chaussées (France) are greatly acknowledged for financing this research project.

LIST OF MAIN SYMBOLS

Latin

$a(t)$	Acceleration time history
c	Soil cohesion
CAV	Cumulative absolute velocity
C_{NN}, C_{VV}, C_{MM}	Imaginary parts of dynamic impedances of the foundation
d	Duration of an acceleration time history
D	Diameter of circular footing
f_{BS}	Bounding surface
g	Acceleration of gravity: $g=9.81$ m/s^2
G	Elastic shear modulus of the soil
h	Plastic modulus
h_0	Numerical parameter used for the definition of h
H	Height of the superstructure
I_A	Arias Intensity
J_F	Mass moment of inertia of the foundation
K_{ij}, $i, j=N, V, M$	Elastic stiffness matrix coefficients
$\tilde{K}_{ij}$, $i=j=N, V, M$	Elastic stiffness matrix coefficients before uplift initiation
K_S	Stiffness of the superstructure in the horizontal translation DOF
m_F, m_S	Mass of the foundation, mass of the superstructure
M	Resultant moment on the footing
$\underline{n}$	Unit normal vector on a surface
$\bar{N}$	Resultant centered vertical force on the footing
N_{max}	Maximum vertical force supported by the footing
PGA	Peak ground acceleration
q_N, q_V, q_M	Dimensionless generalized kinematic parameters
q_S	Dimensionless horizontal translation of the superstructure
q_i^{el}, q_i^{pl}	Elastic and plastic part of the displacement (dimensionless)
Q_N, Q_V, Q_M	Dimensionless generalized force parameters
$Q_{V,max}$, $Q_{M,max}$	Dimensionless maximum horizontal force and moment supported by the footing
$Q_{M,0}$	Moment of uplift initiation (dimensionless)
T	Period
V	Resultant horizontal force on the footing
V_S	Shear wave velocity
V_{La}	Lysmer's analog velocity
u_x, u_z	Horizontal and vertical displacement
u_x^+, u_x^-	Maximum and minimum algebraic values of the footing horizontal displacements
v^+, v^-	Maximum and minimum algebraic values of the ground velocity
W	Weight

Greek

γ	Soil unit weight
θ	Angle of rotation
θ^+, θ^-	Maximum and minimum algebraic values of the footing rotations
l	Measure of the distance between current stress point and its image point
l_{min}	Minimum attained value for the quantity l during the loading history
ν	Poisson's ratio
ξ	Critical damping ratio

Notation

$\underline{a}^T$	Transpose of $\underline{a}$
$\dot{a}$	Time derivative of a
∂a	Boundary of a domain a

REFERENCES

1) Butterfield, R. (1980): A simple analysis of the load capacity of rigid footings on granular materials, *Journée de Géotechnique*, 128–134.
2) Cassidy, M. J., Martin, C.M. and Houlsby, G. T. (2004): Development and application of force resultant models describing jack-up foundation behaviour, *Marine Structures*, **17**, 165–193.
3) Chatzigogos, C. T. (2007): Comportement sismique des fondations superficielles: Vers la prise en compte d'un critère de performance dans la conception, *PhD Thesis*, École Polytechnique, p. 346.
4) Chatzigogos, C. T., Pecker, A. and Salençon, J. (2007): Seismic bearing capacity of a circular footing on a heterogeneous cohesive soil, *Soils and Foundations*, **47**(4), 783–797.
5) Chatzigogos, C. T., Pecker, A. and Salençon, J. (2008): Macroelement modelling of shallow foundations, *Soil Dynamics and Earthquake Engineering*, doi: 10.1016/j.soildyn.2008.08.009.
6) Crémer, C., Pecker, A. and Davenne, L. (2001): Cyclic macro-element for soil-structure interaction: material and geometrical non linearities, *International Journal for Numerical and Analytical Methods in Geomechanics*, **25**, 1257–1284.
7) Crémer, C., Pecker, A. and Davenne, L. (2002): Modelling of nonlinear dynamic behavior of a shallow strip foundation with macroelement, *Journal of Earthquake Engineering*, **6**(2), 175–211.
8) Dafalias, Y. F. and Hermann, L. R. (1982): Bounding surface formulation of soil plasticity, *Soil Mechanics–Transient and Cyclic Loading* (eds. by Pande, G. N., Zienkiewicz, O. C.), Wiley, 173–218.
9) Di Prisco, C., Nova, R. and Sibilia, A. (2003): Shallow footing under cyclic loading: Experimental behavior and constitutive modeling, *Geotechnical Analysis of the Seismic Vulnerability of Historical Monuments* (eds. by Maugeri, M., Nova, R.), Pàtron, 99–121.
10) Eason, G. and Shield, R. T. (1960): The plastic indentation of a semi – infinite solid by a perfectly rough circular punch, *J. Appl. Math. Phys. (ZAMP)*, **11**(1), 33–43.
11) Einav, I. and Cassidy, M. J. (2005): A framework for modelling rigid footing behaviour based on energy principles, *Computers and Geotechnics*, **32**, 491–504.
12) Gajan, S. and Kutter, B. L. (2007): A contact interface model for nonlinear cyclic moment-rotation behavior of shallow foundations, *Proc. 4th Intl. Conf. Earthquake Geotechnical Engineering*, Paper No. 1458, Thessaloniki, Greece, June 25–28 2007.
13) Gazetas, G. (1991): Foundations Vibrations, *Foundation Engineering Handbook* (ed. by Fang, H. Y.), Chapter 15, van Nostrand Reinhold, NY.
14) Gottardi, G., Houlsby, G. T. and Butterfield, R. (1999): Plastic response of circular footings on sand under general planar loading, *Géotechnique*, **49**(4), 453–469.
15) Grange, S. (2008): Modélisation simplifiée 3D de l'interaction sol-structure: application au genie parasismique, *Thèse de Doctorat*, Institut Polytechnique de Grenoble, p. 150.
16) Houlsby, G. T. and Cassidy, M. J. (2002): A plasticity model for the behaviour of footings on sand under combined loading, *Géotechnique*, **52**(2), 117–129.
17) Houlsby, G. T., Cassidy, M. J. and Einav, I. (2005): A generalised Winkler model for the behaviour of shallow foundations, *Géotechnique*, **55**(6), 449–460.
18) Le Pape, Y., Sieffert, J. G. and Harlicot, P. (1999): Analyse non linéaire par macro-éléments du comportement des fondations superficielles sous action sismique, *Comptes Rendus du 5éme Colloque National AFPS*, Cachan, France, 19–21 Octobre 1999, 207–214.
19) Le Pape, Y. and Sieffert, J. G. (2001): Application of thermodynamics to the global modelling of shallow foundations on frictional material, *International Journal for Numerical and Analytical Methods in Geomechanics*, **25**, 1377–140.
20) Martin, C. M. and Houlsby, G. T. (2000): Combined Loading of spudcan foundations on clay: Laboratory tests, *Géotechnique*, **50**(4), 325–338.
21) Mendoza, M. J. and Auvinet, G. (1988): The Mexico earthquake of September 19, 1985 – Behavior of building foundations in Mexico City, *Earthquake Spectra*, **4**(4), 835–852.
22) Nazé, P. A. (2004): Contribution à la prédiction du dommage des structures en béton armé sous sollicitations sismqiques, *PhD Thesis*, INSA Lyon, p. 144.
23) Nova, R. and Montrasio, L. (1991): Settlements of shallow foundations on sand, *Géotechnique*, **41**(2), 243–256.
24) Paolucci, R. (1997): Simplified evaluation of earthquake-induced permanent displacements of shallow foundations, *Journal of Earthquake Engineering*, **1**(3), 563–579.
25) Pedretti, S. (1998): Non-linear seismic soil foundation interaction: analysis and modelling method, *PhD Thesis*, Dpt. Ing. Strutturale, Politecnico di Milano.
26) Randolph, M. F. and Puzrin, A. M. (2003): Upper-bound limit analysis of circular foundations on clay under general loading, *Geotechnique*, **53**(9), 785–796.
27) Saitoh, M. (2007): Simple model of frequency-dependent impedance functions in soil-structure interaction using frequency-independent elements, *ASCE Journal of Engineering Mechanics*, **133**(10), 1101–1114.
28) Veletsos, A. S. and Wei, Y. T. (2001): Lateral and rocking vibrations of footings, *ASCE Journal of Soil Mechanics and Foundations Division*, **97**(9), 1227–1248.
29) Wolf, J. P. (1988): *Soil-Structure Interaction Analysis in the Time Domain*, Prentice Hall Inc., New Jersey.